Optica Applicata, Vol. XLIV, No. 3, 2014
DOI: 10.5277/oa140308

Monitoring and identification of marine oil spills using advanced synthetic aperture radar images

ZAKARYA MIHOUB[1*], ABDELATIF HASSINI[1, 2]

[1]Institute of Maintenance and Industrial Safety, University of Oran, B.P.05, Airport Road Es-Senia, Oran, Algeria

[2]Laboratory of Analysis and Application of Radiation LAAR, Faculty of Physics USTOMB, El M'nouer B.P.1505 Oran, Algeria

[*]Corresponding author: zakaryahse@gmail.com

The aim of this study is to propose and test a new methodology for detection of oil spills in the world oceans from advanced synthetic aperture radar imagery embedded in ENVISAT satellite (ENVISAT-ASAR). The proposed and applied methodology includes four levels: data acquisition, dark spots detection, features extraction and dark spots classification for discrimination between oil spills and look-alikes. Level 1 contains the ENVISAT-ASAR wide swath mode data acquisition. Level 2 begins with a visual interpretation based on experience and *a priori* information concerning location, external information about weather conditions, differences in shape, and contrast to surroundings between oil spills and look-alikes, then filtering and segmentation. Level 3 contains extraction of features from the detected dark spots. Level 4 aim is to discriminate oil spills from look-alikes using the features extracted by means of object-based fuzzy classification. As a result, oil slicks are discriminated from look-alikes with an overall accuracy classification of 91% for oil slicks and 86% for look-alikes. Finally, to validate our results, the method has been tested by comparing the areas of the automatically detected oil spills (object-based fuzzy classification) with the areas of the manually detected oil spills (region of interest), by means of area ratios.

Keywords: sea pollution, remote sensing, oil spills detection, ENVISAT-ASAR images.

1. Introduction

Oil slicks on sea surface can have different sources such as man-made slicks from illegal discharges of ships or spills resulting from ship accidents, slicks originated from biological activities such as photo-oxidation processes or by planktons, and geological slicks originated as natural hydrocarbon seeps from a reservoir. Including every kind of slick, 10% of ocean surface is estimated to be covered by slicks [1]. Natural seepage detection is considered to be one of the significant preliminary works for offshore petroleum exploration. However, it does not explain the whole petroleum system by

itself, and it should be combined with regular exploration techniques such as seismic interpretation, sample collection from the sea bottom, and geological survey. The oil slick detection and mapping are becoming one of the standard tools for hydrocarbon exploration activities and have been applied to most of the hydrocarbon basins in the world such as Gulf of Mexico [2], Santa Barbara Channel, California [3], Australian Shelf [4], and South Caspian Sea [5].

Radar systems are extensively used for the dark formation detection in the marine environment, as they are not affected by local weather conditions and cloudiness and work day and night [3]. They emit their own energy in the microwave range, which is then reflected from the sea surface and received back at the sensor. A radar image is a representation of the backscatter return and is mainly proportional to the surface roughness at the scale of the radar wavelength (few centimeters) [6]. Synthetic aperture radar (SAR) capabilities are widely well demonstrated, and thus it still turns out to be the most efficient and superior satellite sensor in oil spill detection [7]. Parameters used to detect oil slicks are functions of radar configuration, slick nature, meteorological and oceanic conditions like the height of the waves, the amount of oil that has been released, and the speed of the wind [1, 8]. SARs have some limitations, as the presence of natural phenomena that can give false oil spill detections (look-alikes), such as oil spills from oil-rigs, leaking pipelines, passing vessels as well as bottom seepages, while look-alikes do include natural films/slicks, grease ice, threshold wind speed areas (wind speed <3 m/s), wind sheltering by land, rain cells, shear zones, internal waves, *etc.* [8].

Detection of oil spills from SAR imagery can be divided into three steps: 1) detection of dark spots (suspicious slicks), 2) extraction of features from the detected dark spots, and 3) classification of the dark spots (oil spills/look-alikes) [7]. This can be done manually or automatically. In manual detection, a trained operator has to go through the entire image, find possible oil spills and discriminate between the oil spills and the look-alikes. Though a trained operator is able to detect oil spills from SAR images with some confidence, it is time-consuming. It is also labor-intensive given the large number of SAR images that must be analyzed in a short period of time for effective oil-spill monitoring, especially after the launch of constellations like Sentinel-1A and 1B and the RCM (RADARSAT Constellation Mission). For some areas and in sight of a local ground station, products can be delivered within one hour [9]. The first Sentinel-1A satellite was launched on April 3, 2014, it will ensure the continuity of the C-band SAR data from the ERS-1/2 and ENVISAT missions, with the second Sentinel 1-B following in 2016. For further reading ESA websites are recommended (https://earth.esa.int/web/guest/missions/esa-future-missions/sentinel-1). In addition, manual detection is constrained by the knowledge and experience of operators, whose results are subjective.

Discriminative features of oil spills and look-alikes are basically geometrical, radiometric, textural, and temporal [7, 10]. Natural oil slicks originated from subsurface should be permanent, and temporally many different slicks should be present in a close

neighborhood with a repetitive manner. However, orientation, shape, and texture can be different because of the weather conditions at the time of image acquisition [10, 11]. Thus, studies have been undertaken to develop fast, reliable and automated oil-spill detection systems. Several classifiers have been employed for the discrimination of oil spills and look-alikes: Bayesian classification scheme by combining prior knowledge, Gaussian densities and rule-based density corrections [12, 13], linear discriminate analysis (LDA) approach basing on the Mahalanobis distance [14], a multiple linear regression method for oil-spill classification [15], the artificial neural network (ANN) approach to approximate the relation between dark-spot features and the class labels [16], the support vector machine (SVM) [17], object-based fuzzy classification [11], bundling, bagging, boosting and the generalized additive model (GAM) [18].

In this paper, we propose a multi-level methodology for detection of oil slicks using ENVISAT-ASAR imagery and apply our methodology in a variety of conditions, including different regions of the planet, and different dates. We establish that the method can be used to support the identification of hydrocarbon seeps.

2. Materials – satellite sensor description and input data

Microwave sensors are the most applicable tools for oil slick monitoring since they are not affected by clouds, haze, weather conditions, and day/night differences. Synthetic aperture radar is the most common method to detect offshore oil slicks. Parameters used to detect oil slicks are functions of radar configuration, slick nature, meteorological and oceanic conditions like the height of the waves, the amount of oil that has been released, and the speed of the wind [1, 19].

The advanced synthetic aperture radar (ASAR) sensor rides aboard the ENVISAT satellite and provides radar imagery of the earth for studying oceans, atmosphere, ice, and land [19]. ASAR was operational since the launch of the satellite on March 1, 2002 [19, 20], and the mission operated until April 8, 2012 [20]. The processing and archiving of data from ESA's (European Space Agency) ERS-2 and ENVISAT missions were unified in the ESA multi-mission facility infrastructure (MMFI). Since then the MMFI served both missions until their end, for ERS-2 in July 2011 and ENVISAT in April 2012. Nevertheless, the mission data are still being archived and are frequently requested by users, with MMFI still serving those needs. It and the attendant processing were transferred from the former mission-specific payload ground segments to a modern processing infrastructure [21].

ASAR has five mutually exclusive modes of operation: image mode (IM), alternate polarization (APM), wide swath (WSM), wave (WM), global monitoring (GMM). Image mode, has 30 m resolution, similar to ERS SAR, 7 possible mutual exclusive swaths and 2 possible mutual exclusive polarizations (VV or HH). Alternate polarization mode, has 30 m resolution, 7 possible mutual exclusive swaths and 3 possible mutual exclusive polarizations (HH/VV, HH/HV or VV/VH). Wide swath mode, 150 m

resolution, has 1 unique swath (400 km) and 2 possible mutual exclusive polarizations (VV or HH) [22]. In the literature, for oil slick detection VV polarized, C-band with low incidence angle data is considered preferable [1, 8, 23–25]. The methodology proposed has been applied on a dataset of 10 ENVISAT-ASAR images of wide swath mode (WSM) [26].

3. Methods

The proposed and applied methodology in this study is an implementation of pre-existing techniques, with a new approach, to 4 differing contextual levels, as shown in Figure 1:

– ENVISAT-ASAR data acquisition,
– dark spots detection,
– feature extraction from the detected dark spots,
– classification of dark spots to discriminate oil spills from look-alikes.

3.1. Level 1: ENVISAT-ASAR data acquisition

The ENVISAT-ASAR data are downloaded from the ESA (European Space Agency) websites (https://earth.esa.int/web/guest/data-access) [26]. In this study, the wide

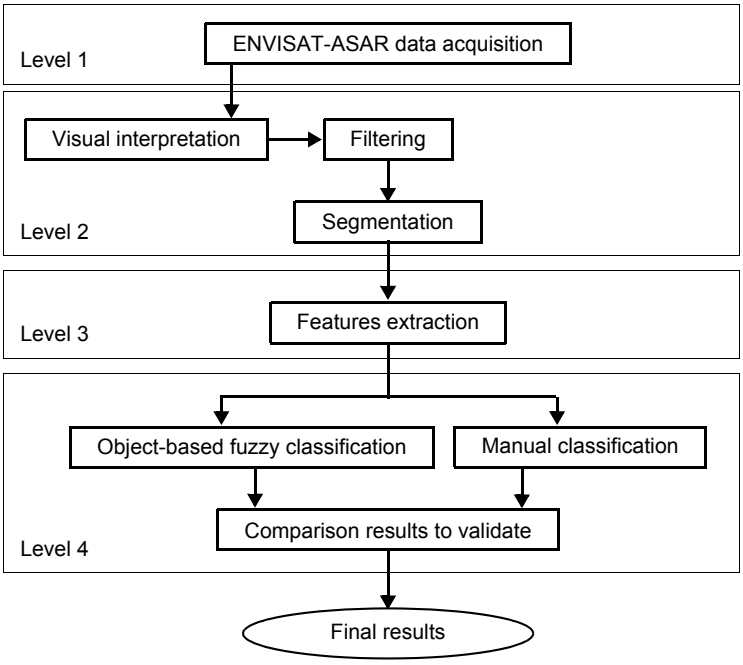

Fig. 1. Representative framework of the methodology.

T a b l e 1. List of images used.

Environment	Date and time of acquisition	Region
Image A (image reference)	17/11/2002 at 10:44 UTC	Northwest coast of Spain
Image B	25/11/2011 at 12:12 UTC	Northeast of Rio De Janeiro Brazil coast
Image C	28/04/2010 at 03:45 UTC	Gulf of Mexico
Image D	09/05/2010 at 15:48 UTC	Gulf of Mexico
Image E	27/08/2008 at 09:20 UTC	Northeast coast of Algeria
Image F	31/03/2005 at 12:13 UTC	Coast of South Africa
Image G	07/12/2007 at 01:40 UTC	South Korea coast
Image H	30/07/2004 at 20:08 UTC	Southeast of the Baltic Sea
Image I	09/08/2006 at 09:54 UTC	Lebanese coast
Image J	10/04/2004 at 01:55 UTC	East China Sea

swath mode, level 1b ASA_WSM_1P are used. The study area is covered by 10 different ENVISAT-ASAR images. The details of the dataset containing the information about the region, date and start time of acquisition are given in Table 1.

3.2. Level 2: dark spots detection

The capability of ASAR in detecting oil slicks over the sea surface is well-known and proven by several studies aiming at oil spill detection and discrimination using ENVISAT-ASAR images [1, 6, 7, 13, 17, 27, 28]. Most of these studies are primarily based on the dark spots detection; it is a preliminary task when detecting oil spills; it is a critical and fundamental step prior to feature extraction and classification. Therefore, unless an oil spill can be detected at this first step, it can never be detected at a later step. Furthermore, the accuracies of feature extraction and classification greatly rely on the accuracy of dark-spot detection. This level includes three steps.

Visual interpretation – Visual interpretation starts with a pre-processing stage where artifacts (if applicable) resulting in different contrast trends across the images (range falloff, gain control effects, *etc*.) have been determined and removed [29]. The de-trended images with balanced contrast have been scanned visually to determine the target dark spots. The human eye is superior in observing a slick in the context of the surrounding sea, and a trained human interpreter can discriminate oil slicks and look-alikes based on experience and *a priori* information concerning location, external information about weather conditions, differences in shape, and contrast to surroundings between oil slicks and look-alikes [12]. If the surroundings are homogeneous, the human observer will have more belief in that the spot is an oil slick than with heterogeneous surroundings [12]. With heterogeneous surroundings, the human eye can easily determine if the spot is separated from the surroundings based on contrast or orientation [27]. In this study the images have been thoroughly analyzed by different

experts using visual photo-interpretation techniques, furthermore the subset images are extracted based on target areas containing dark spots on the bases of contrast level to the surroundings, homogeneity of the surroundings, wind patterns, nearby bright spots of ships, edge, and shape characteristics for natural slicks. Closely spaced, a number of dark spot groups or large individual ones are limiting the subsets spatially.

Filtering – Image filtering step aims to reduce speckle and to enhance the image [30]. Adaptive filtering methods are used to discriminate high contrast areas representing possible oil discharges in the images. In general, the filter of image with noise removal: Lee, Gamma, Frost or Kuan and two pass filters (3×3 median filter and 5×5 low pass filter) are used in different oil spill discrimination studies [31, 32]. It is also observed that these filters minimize the loss of information boundaries of high and low contrasted areas. Filtering of the image with noise removal filters gives a clear output for discrimination of dark areas from the remaining heterogeneous background [19, 33]. In this study the Lee (3×3) filter is used.

Thresholding and segmentation – In segmentation neighboring pixels are compared and they are merged into regions if they are similar. It runs iteratively to merge the resulting regions. Two neighboring regions, R_i and R_j, are merged if they satisfy the three following conditions:

1. Thresholding condition: $\text{dist}(R_i, R_j) \leq T$;
2. Neighborhood condition 1: $R_j \in N(R_i)$ and $\text{dist}(R_j, R_i) \leq \text{dist}(R_k, R_i), R_k \in N(R_i)$;
3. Neighborhood condition 2: $R_k \in N(R_i)$ and $\text{dist}(R_i, R_j) \leq \text{dist}(R_k, R_j), R_k \in N(R_j)$.

In the above, T is the chosen similarity threshold, $\text{dist}(R_i, R_j)$ is the Euclidean distance between the mean grey levels of the regions. Also, regions smaller than the chosen area threshold are removed by merging them with their most similar neighbor [34]. In this approach, a detection window is passed through the ASAR image. An intensity threshold segmentation algorithm is implemented for each window. Pixels with intensities below the intensity threshold are regarded as potential dark-spot pixels while the others are potential background pixels [35].

3.3. Level 3: features extraction for dark spots

After segments have been created, features need to be extracted as an input to classifiers. The features proposed by the researchers can be categorized into four groups: 1) physical and textural properties, 2) geometric shape, 3) contrast with background, and 4) contextual information [7]. Different researchers employed different features. For example, TOPOUZELIS *et al*. (2007) adopted 10 features to train a neural network classifier [16], FISCELLA *et al*. (2000) used 11 features [14] and SOLBERG *et al*. (2007) used 13 features [13].

Although most classifiers relied predominantly on limited features, they tended to present different patterns on feature ranking and permutation-based variable accuracy importance (PVAI) values [18]. The importance of a variable may show great variation, depending on which evaluation criterion is used. As a result, features that are useless for a particular classifier may be of great help for another, while features that are useful for one classifier may become useless for another. Some shape features and a contex-

tual feature have very high PVAI values in most of the classifiers [18]. In this study, we intend not to use all the features proposed by other researchers, because it will increase the dimensionality of the dataset, thus the risk of over fitting. Therefore, we select 11 features out of all the available features as a classifier input. The selected 11 features related to: intensity value of pixels (layer values) (predictors no. 1 to 3), shape (no. 4 to 7), to texture (no. 8 to 11) [27], see Table 2.

T a b l e 2. Summary statistics of features for oil spills and look-alikes separately.

No.	Features	Oil spill (min–max)	Look-alikes (min–max)
1	OSd	8.1–42.2	31.5–71.8
2	BMe	31.6–161.7	42.2–194.0
3	BSd	10.1–56.6	21.5–76.1
4	*A*	17–16.619	325–170.384
5	*P*	64–2011	106–2807
6	$C = P^2/A$	20.4–510.8	15.2–325.9
7	Com	2.1–2.4	1.5–2.5
8	*S*	72.1–100	54.9–99.9
9	*H*	0.024–0.040	0.038–0.042
10	Con	1.324–2.140	1.230–1.690
11	*D*	25–35	23–27

OSd – standard deviation of gray-scale intensity values of the object; BMe – average intensity value of the background area; BSd – standard deviation of the intensity value of the background; *A* – target area (in number of pixels); *P* – target perimeter (in number of pixels); $C = P^2/A$ – complexity measure; Com – compactness; *S* – spreading measure (the ratio between the target width and length); *H* – homogeneity; Con – contrast; *D* – dissimilarity.

The selected features in this study are used for defining the boundaries of the membership functions while making object-based fuzzy classification [27]. The index parameters are selected to identify the geometric shape of the dark spot and spectral similarity of the neighboring pixels (background). Features related to shape (*A*, *P*, *C*, Com and *S*) are defining the geometric properties of the dark spot, because the dark spot related with natural oil slicks should have larger width with respect to slicks created by oil tankers or large ships. Similarly they should have less rounded shapes with respect to low-wind areas and the algae or biological dampening effects. Secondly, features related to texture (*H*, *C* and *D*) and intensity value of pixels (OSd, BMe and BSd) are used to define spectral properties of dark spots.

3.4. Dark spots classification

This level includes two steps: 1) automatic classification (object-based fuzzy classification) and 2) manual classification (region of interest).

Automatic classification (object-based fuzzy classification). Several classifiers have been used for classification of dark formations to oil spills or look-alikes, *i.e.*, statistical approach through computation of probabilities, neural networks, fuzzy logic, *etc*.

The last stage includes defining membership functions based on extracted object features [10]. In this paper an object-based fuzzy classification scheme is used for discriminating dark spots, with a simple empirical class hierarchy consisting of two classes which are "clear sea water" and "dark spots". "Dark spots" class includes two subclasses, namely "probable oil slicks" and "probable look-alikes". Fuzzification describes the transition from a crisp system to a fuzzy system. The fuzzy rule can have a single condition or can consist of a combination of conditions that have to be fulfilled for a dark object to be assigned to a probability class [11]. A membership function assigns a membership degree or value between 0 and 1 to each feature. Boundaries of membership functions are determined based on feature value intervals from randomly selected representative segments that are supposed to belong to a specific class. In most of the cases, "Boolean range function" is used, which assigns a value of "1" between specific values and assigns "0" for the rest, in order to achieve sharp distinction of "probable oil slick" and "probable look-alike" classes [27]. As a final stage of this classification, an accuracy assessment is performed by classification stability (CS) and best classification result (BCR) methods, apart from comparisons of level 1 visual interpretation results. CS explores differences in degrees of membership between the best and the second best class assignments of each object, which can give evidence about the ambiguity of an object's classification. On the other hand, BCR determines whether the object has memberships in more than one class. In the accuracy assessment of classification schemes, basic statistical information describing the classes like number of image objects, mean, standard deviation, minimum value, and maximum value has been calculated [27].

Manual classification (region of interest). Regions of interest (ROIs) are portions of images, either selected graphically or selected by other means such as thresholding. The regions can be irregularly-shaped and are typically used to extract statistics for classification, masking, and other operations. ENVI (the Environment for Visualizing Images, Research Systems, Inc., Boulder, USA) allows selection of any combination of polygons, points, or vectors as a region of interest. Multiple regions of interest can be defined and drawn in any of the main image, scroll, or zoom windows. Regions of interest can be grown to adjacent pixels that fall within a specified pixel value threshold. As done for the training dataset, each oil spill signature present in ENVISAT--ASAR data was manually digitized via ENVI's region of interest (ROI) tool and saved to oil spill position text files. ROIs were used as reference oil spill regions [6, 26, 28]. Lastly, to validate our results, the methodology has been tested with computing a success percentage by comparing the areas of the automatically detected oil spills with the areas of the manually detected oil spills, by means of area ratios.

4. Results and discussion

In our case, we have used wide swath mode level 1b images with spatial resolution of 150 m. This class of filenames begins with the following convention: ASA_MOF_1PXPDEyyyymmdd_hhmmss, where ASA denotes the sensor (ASAR),

MOF is the functioning mode (IM, APM, WSM, WM, GMM), yyyymmdd is the year, the month (01–12) and the day (01–31), respectively, hh is the hour (UTC) when the sensor began collecting the scene's data (00–23), mm is the minute (00–59), and ss is the second (00–59).

Image A (reference image) is used to process oil spill pixels covering the Spain Coast from the Prestige accident (2002). Because of the important number of oil spill pixels on this image, it is considered like the reference image in this work (image A of Fig. 2). The file of this image named ASA_WSM_1PXPDE20021117_104431_000000672011_00180_03741_0009.N1 was received from an official source (https://earth.esa.int/web/guest/data-access). In this case, our image was received on the 17/02/2002 at 10:44:31 UTC, with wide swath mode, 00180 frame number and 03741 orbit number.

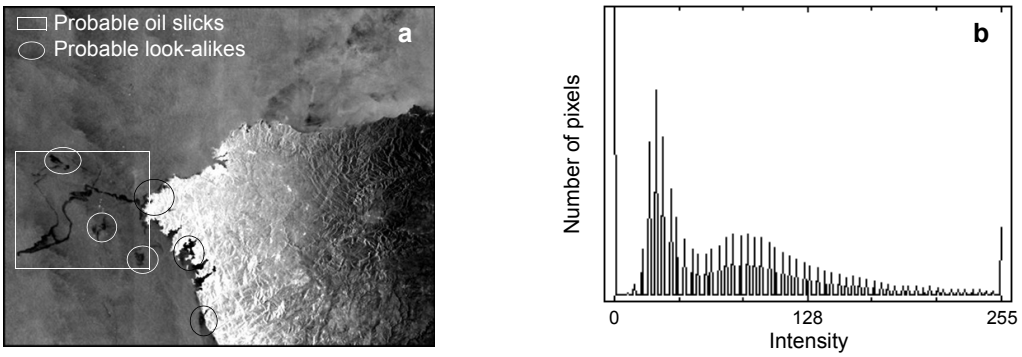

Fig. 2. Visual analyses of the image A (**a**), and the histogram (**b**).

The other event, on November 14, 2011; US energy giant Chevron said Monday it has suspended drilling following an oil spill in waters off Rio de Janeiro state. The image of this event (image B of Fig. 3) is acquired by an advanced synthetic aperture radar (ASAR) sensor from the ENVISAT satellite, and covers the oil spill pixels

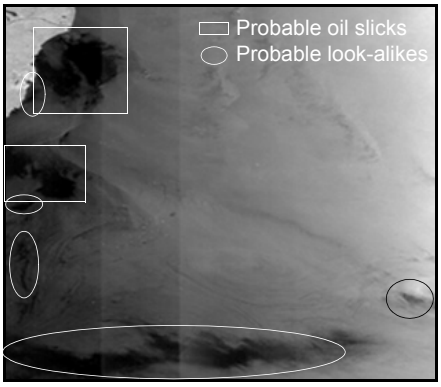

Fig. 3. Visual analyses of the image B.

in the northeast coast of Brazil. The file of this image named ASA_WSM_1PXPDE20111125_121304_000026293109_00052_50928_0009.N1 was acquired on November 25, 2011 with wide swath mode, 00052 frame number and 50928 orbit number at 12:13:04 UTC. This image is used to corroborate our research.

Firstly, in the visual interpretation step, the ten images are manually interpreted and Lee 3×3 noise removal filter is applied. Filtering of the image with noise removal filters gives a clear output for discrimination of dark areas from the remaining heterogeneous background. ASAR imagery is highly speckled and the dark spot may have different contrasts relative to its background under different conditions. If the spatial distribution of intensity is considered, the dark spot and the background can be separated further. Before addressing this idea in detail, it is necessary to clarify our terminology to avoid any confusion [35].

In this paper, pixels with intensities below the intensity threshold are referred as "probable dark-spot pixels" or "dark pixels". Pixels with intensities above the intensity threshold are referred as "probable background pixels" or "light pixels". For each image, we used the histogram to present intensity pixels distribution for each image combination selected (number of pixels/intensity [0–255]), and to define the density (number of pixels) of different intensity pixels (dark and light). We can observe that dark pixels distribution in Fig. 2**b** (histogram of image A) presents a larger part compared to light pixels, especially for the values in the range 20–50, because of the important number of dark spots in image A.

We applied these interpretations on other images (image B to image J in Table 1) and the results are shown in Fig. 4. Based on these interpretations, 21 subset images are selected and 65 dark spots are detected to be investigated in further stages. Figures 2 and 3 present the visual analyses of images A and B, respectively; the square presents possible oil slicks and the ellipse presents the possible look-alike.

For the segmentation of images, the segment scale parameter is decided as 20 after several trials. Shape factor is set to 0.4. Smoothness parameter is set to 0.7 yielding compactness to be automatically 0.3. Figures 5**a** and 6**a** present the detection of dark spots to identify the oil spill pixels from image A and B, respectively, using automatic

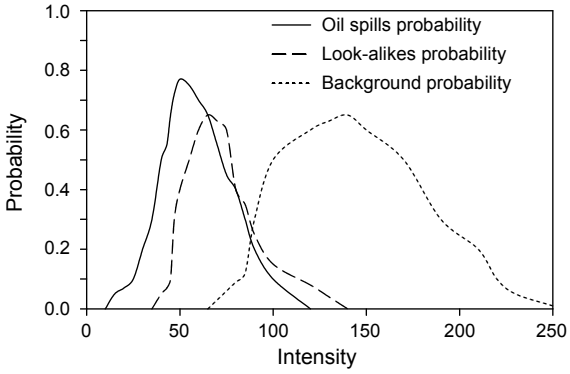

Fig. 4. Probability of detecting oil spills, look-alikes and background.

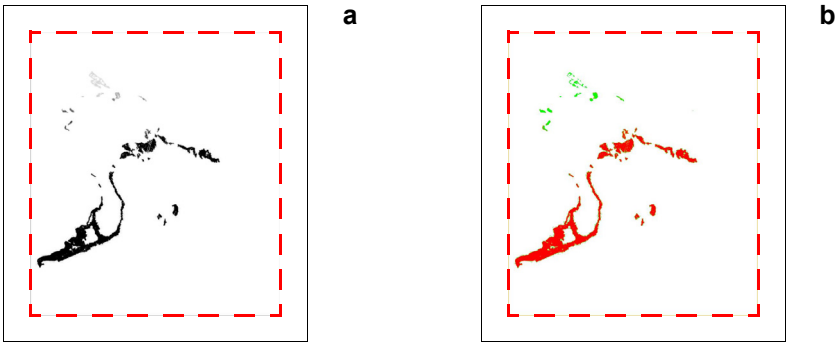

Fig. 5. Segmented subset image, simple scene for image A (**a**), representing the discrimination of two dark spot classes (**b**).

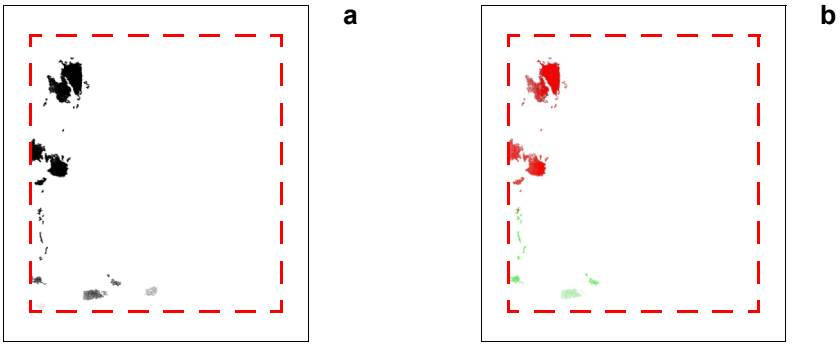

Fig. 6. Segmented subset image, simple scene for image B (**a**), representing the discrimination of two dark spot classes (**b**).

segmentation conditions 1–3. We can observe a number of dark spots detected. Major part of these dark spots detection problem is found to be connected with distinguishing oil spills from other natural phenomena (look-alikes), *e.g.*, low wind area, wind front area and natural slicks that create dark patches in ENVISAT-ASAR images.

After segmenting subsets images, the specific features related to "layer values", "shape", and "texture" are automatically calculated for each segment. Sample segments are selected randomly, which are supposed to belong to one specific class. The interval of feature values is determined and tabulated, as shown in Table 2.

Based on the extracted features tabulated (Table 2), the membership functions are defined for the class hierarchy. For class "dark spot", a Boolean range membership function is defined using standard deviation of gray-scale intensity (OSd) values. Since "probable oil slick" and "probable look-alike" classes are subclasses of "dark spot" class, this membership function appears to be an inherited function for them, and the rules are valid for the subclasses as well. The image is classified based on the membership functions, but some segments are found to be unclassified. In order to correct the unclassified areas, the membership function and logical operators are modified and

tweaked for intersecting boundaries of feature values. At last, the resultant classified image is obtained. The applied methodology combines pixel-based filtering, supervision of human interpreter, object-based segmentation, and fuzzy classification. In object-based classification, the pixels are grouped to segments based on the two different input data. Membership functions helped to adjust the specific character of every individual subset. The algorithm converts every segment to a binary object with the help of Boolean range membership functions.

Standard deviation of gray-scale intensity (OSd) values in image A are in the range 0–255 where the oil spills values are 7.3–40.1 and the look-alikes are 32.3–70.3, and on other hand, OSd values in image B are in the range 0–255, where the oil spills values are 10.1–54.3 and the false alarms are 33–69.2. Starting from the OSd values and the target area (A), we can estimate the oil spill (OS) quality and quantity, for example from image A, the number of common OSd values between the oil spill and false alarms is small, so it is easy to discriminate between them because of the big quantity of a heavy oil spill (Prestige accident). But in image B the common OSd values interval is large because of the small quantity of an oil spill (natural or operational oil spill causes). In addition to that, we can estimate the look-alikes nature, such as low wind, wind front, *etc*.

Figure 5**b** presents classification results for the subset image A and Fig. 6**b** for the image B, representing the discrimination of two dark spot classes (oil slicks and look-alikes). Oil spills locations have been enhanced and edged in red color, green color presents probable look-alikes and white color presents clear sea water.

For the accuracy assessment, CS and BCR method is used to evaluate the accuracy of the classes. In this respect, the classification accuracy is calculated from CS and BCR, in which they show the basic statistics and probability of segments belonging to the classes that they are assigned by the fuzzy logic defined by the membership functions. Since there is neither training set for class definition nor control set for absolute accuracy assessment, only the consistency of classes within themselves could be measured. However, it should be kept in mind that there is always a risk of obtaining wrong results even if class stability results show high level of consistency.

As a result of "classification stability", 89 segments out of 9.527 are classified as "probable oil slicks" with an accuracy of 91%, 191 segments are classified as "probable look-alikes" with an accuracy of 86% and 9.092 segments are classified as "clear sea water" with an accuracy of 96%. Moreover, BCR showed that 97% of segments belonging to "probable oil slicks" has only one class; similarly, probability of segments belonging to "probable look-alikes" and "clear sea water" are 96% and 98%, respectively.

As done for the training dataset, each oil spill signature presents in ENVISAT-ASAR data was manually digitized via ENVI's ROI tool and saved to oil spill position text files. ROIs were used as reference oil spill regions. Dark formations are usually classified as potential oil spills according to the following criteria: dark homogeneous spots in a uniform windy area and linear dark areas, not extremely large, with abrupt turns. And they are usually classified by visual interpretation as look-alikes according

to the following criteria: low wind areas; coastal zones due to wind sheltering and elongated dark areas with smooth turnings in spiral shape [26, 28].

Lastly, to validate our results, the methodology has been tested with computing a success percentage by comparing the areas of the automatically detected oil spills with the areas of the manually digitalization of oil spills via ROI, by means of area ratios.

An example of this procedure is shown in Figs. 7 and 8 from image A and B, respectively. Figures 7 and 8 show the representative steps to validate the oil spills detection methodology. The input images (image A and B) contain oil spills to be detected. Applying the oil spills automatic detection (fuzzy classification) to the inputs image, we obtain the result shown in Figs. 7**a** and 8**a**, where black regions in red ellipse/square represent all candidate oil spills and green ellipse represents look-alikes. Manual digitalization of the oil spill (ROI) is shown in Figs. 7**b** and 8**b**, depicted by the green region. Finally, Figs. 7**c** and 8**c** show the comparison result in terms of an area ratio by the percentage of success, red pixels are common pixels belonging to both automatic detected pixels (in red ellipse (**a**)) and manually digitized pixels (in green region (**b**)).

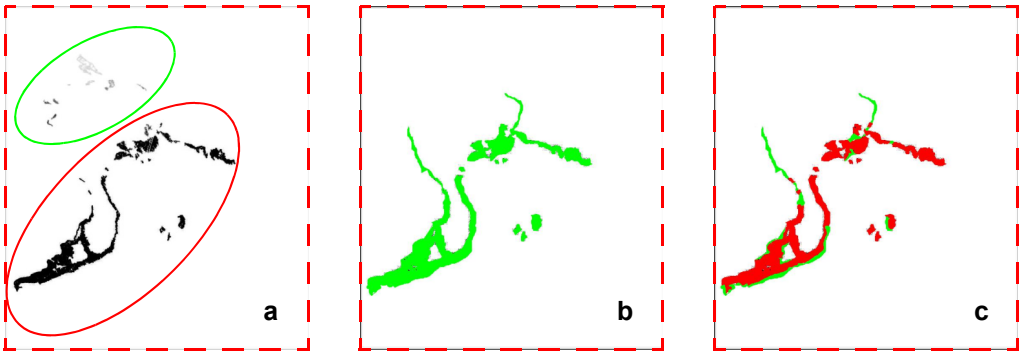

Fig. 7. Comparison result (**c**) of automatic classification (fuzzy classification) (**a**), and manually digitalized (ROI) (**b**) from image A.

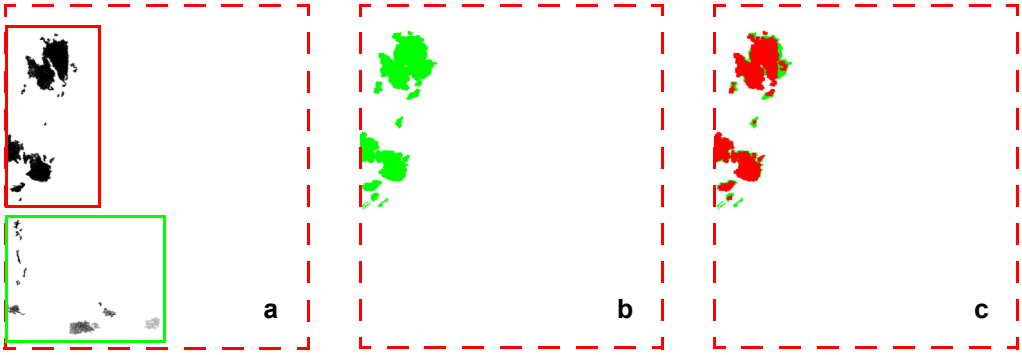

Fig. 8. Comparison result (**c**) of automatic classification (fuzzy classification) (**a**), and manually digitalized (ROI) (**b**) from image B.

Figures 7**c** and 8**c** show that oil pills areas detected by the algorithm are in general different than those manually digitalized.

This is not surprising since the manual digitalization of an expert operator can often include water pixels at the border of an oil spill contour and can connect disjoint regions separated by few pixels. This implies an overestimation of the actual area covered by the oil and a subsequent decreasing in the success percentage. The area ratio percentage is 93% and 90% from image A (reference image) and B, respectively, so the applied methodology can discriminate oil spills from look-alikes with good percentage in these images (image A and B). The proposed oil spill classification method is tested with eight other scenes of images (image C to image J in Table 3).

T a b l e 3. Area ratio comparison procedure applied to the validation oil spills (OS) dataset.

Location/OS source	Number of subset images	OS area/ROI area
Image A	2	93%
Image B	3	91%
Image C	2	83%
Image D	2	84%
Image E	1	78%
Image F	3	79%
Image G	2	80%
Image H	2	91%
Image I	1	77%
Image J	3	89%
Total	21	84.5%

Table 3 summarizes results of the application of the procedure described above to the entire validation dataset of 89 oil spills. The overall percentage of correct identification of the area covered by the 21 subset images analyzed is 84.5%. In general, these results are very encouraging and promising, because the method can detect maximum pixels of dark spots pixels and discriminate oil slicks from look-alikes.

In some images, the percentage of correct identification is obviously lower than the percentage derived analyzing only the number of identified regions. Since this method compares the overall area classified as oil by the automatic system with the ROI area for each event, the limited decrease in percentage resulting from Table 3 indicates that the system detected the presence of oil region despite the ambiguity of the area in which oil and water are not really separated in some subsets.

On the one hand, the smallest values are observed in some images (*e.g.*, image E: 78%, image F: 79%, image I: 77%), because of:

– a small area of oil spills in this scene of image (operational or natural causes),

– a large area of look-alikes caused mainly by biogenic slicks and low-wind areas (less than 3 m/s or superior to 12 m/s).

On the other hand, the largest values are observed in a number of images (*e.g.*, image A: 93%, image B: 91%) because of the important number of oil spill pixels in these images (accidental causes).

5. Conclusion

This paper presents an overview of environmental phenomena: oil spills. SAR sensors are commonly used by oil spill monitoring systems due to their well demonstrated capability of detection. ASAR deployed on satellites is today an important tool in oil spill monitoring due to its wide area coverage and day and night all-weather capabilities. In this paper, an adapted methodology for detection of oil slicks in ENVISAT-ASAR images is presented.

Major part of the oil slick detection problem is found to be connected with distinguishing oil slicks from other natural phenomena that create dark patches in the ENVISAT-ASAR image. The methodology worked satisfactorily in different cases of oil slicks, by combining different approaches. The discriminative power of human interpreter at the starting phase with the optimization of sea state conditions through noise removal filters yielded a good basis for further segmentation steps. False classifications due to pixel-based approaches are minimized with the object-based approach, and further discrimination between oil slicks and look-alikes became applicable through segmentation, fuzzy membership functions, and classification algorithms. The accuracy of classification is different for different images. The overall accuracy obtained by averaging 21 subsets of 10 images is 91% for oil slicks, 86% for look-alikes and 96% for clear sea water.

Finally, we tested and validated the proposed methodology with computing a success percentage by comparing the areas of the automatically detected oil spills (fuzzy classification) with the areas of the manually digitalization of oil spills (region of interest) by means of area ratios. Using an independent dataset of 89 oil spills events, the overall percentage of correct identification of the area covered by 21 subsets analyzed is 84.5%. We have established that the method can detect the maximum of dark spots pixels and discriminate oil slicks from look-alikes

There are some efforts which must be undertaken in future works. They are as follows:

– An improvement of our results with in situ measurements to validate our work;

– A comparative study of different classification techniques;

– A comparative study between ASAR and optical sensors (*e.g.*, SeaWiFS, MODIS), to eliminate look-alikes from ASAR images;

– How to use classification results (possible oil spills) in the alert system of oil spills.

Acknowledgements – This work is performed as a part of a PhD study funded by the Institute of Maintenance and Industrial Security, University of Oran, Algeria. The authors would like to thank the European Space Agency (ESA), for the ASAR scenes used for illustration purposes.

References

[1] GIRARD-ARDHUIN F., MERCIER G., GARELLO R., *Oil slick detection by SAR imagery: potential and limitation*, [In] *OCEANS 2003, Proceedings*, Vol. 1, 2003, pp. 164–169.

[2] FRIEDMAN K.S., PICHEL W.G., CLEMENTE-COLON P., XIAOFENG LI, *GoMEx – an experimental GIS system for the Gulf of Mexico region using SAR and additional satellite and ancillary data*, [In] *IEEE International Geoscience and Remote Sensing Symposium, IGARSS '02*, Vol. 6, 2002, pp. 3343–3345.

[3] LEIFER I., LUYENDYK B., BRODERICK K., *Tracking an oil slick from multiple natural sources*: *Coal Oil Point, California*, Marine and Petroleum Geology **23**(5), 2006, pp. 621–630.

[4] O'BREIN G.W., LAWRENCE G.M., WILLIAMS A.K., GLENN K., BARRETT A.G., LECH M., EDWARDS D.S., COWLEY R., BOREHAM C.J., SUMMONS R.E., *Yampi Shelf, Browse Basin, North-West Shelf, Australia: A test-bed for constraining hydrocarbon migration and seepage rates using combinations of 2D and 3D seismic data and multiple independent remote sensing technologies*, Marine and Petroleum Geology **22**(4), 2005, pp. 517–549.

[5] WILLIAMS A., LAWRENCE G., *The role of satellite seep detection in exploring the South Atlantic's ultra deep water*, [In] Schumacher D., LeSchack L.A. [Eds.], *Surface Exploration Case Histories: Applications of Geochemistry, Magnetics and Remote Sensing*, AAPG Studies in Geology No. 48, SEG Geophysical References Series No. 11, 2002, pp. 327–344.

[6] PISANO A., *Development of oil spill detection techniques for satellite optical sensors and their appilcation to monitor oil spill disharge in the mdditeranean sea*, PhD Thesis, Department of Control and Management of Natural Resources, University of Bologna, Italy, 2011.

[7] BREKKE C., SOLBERG A.H.S., *Oil spill detection by satellite remote sensing*, Remote Sensing of Environment **95**(1), 2005, pp. 1–13.

[8] ESPEDAL H.A., *Detection of oil spill and natural film in the marine environment by spaceborne synthetic aperture radar*, PhD Thesis, Department of Physics, University of Bergen and Nansen Environment and Remote Sensing Center, Norway, 1998.

[9] HORNÁČEK M., WAGNER W., SABEL D., HONG-LINH TRUONG, SNOEIJ P., HAHMANN T., DIEDRICH E., DOUBKOVÁ M., *Potential for high resolution systematic global surface soil moisture retrieval via change detection using Sentinel-1*, IEEE Journal of Selected Topics in Applied Earth Observations and Remote Sensing **5**(4), 2012, pp. 1303–1311.

[10] TOPOUZELIS K.N., *Oil spill detection by SAR images: dark formation detection, feature extraction and classification algorithms*, Sensors **8**(10), 2008, pp. 6642–6659.

[11] KARATHANASSI V., TOPOUZELIS K., PAVLAKIS P., ROKOS D., *An object-oriented methodology to detect oil spills*, International Journal of Remote Sensing **27**(23), 2006, pp. 5235–5251.

[12] SOLBERG A.H.S., STORVIK G., SOLBERG R., VOLDEN E., *Automatic detection of oil spills in ERS SAR images*, IEEE Transactions on Geoscience and Remote Sensing **37**(4), 1999, pp. 1916–1924.

[13] SOLBERG A.H.S., BREKKE C., HUSØY P.O., *Oil spill detection in radarsat and envisat SAR images*, IEEE Transactions on Geoscience and Remote Sensing **45**(3), 2007, pp. 746–755.

[14] FISCELLA B., GIANCASPRO A., NIRCHIO F., PAVESE P., TRIVERO P., *Oil spill detection using marine SAR images*, International Journal of Remote Sensing **21**(18), 2000, pp. 3561–3566.

[15] NIRCHIO F., SORGENTE M., GIANCASPRO A., BIAMINO W., PARISATO E., RAVERA R., TRIVERO P., *Automatic detection of oil spills from SAR images*, International Journal of Remote Sensing **26**(6), 2005, pp. 1157–1174.

[16] TOPOUZELIS K., KARATHANASSI V., PAVLAKIS P., ROKOS D., *Detection and discrimination between oil spills and look-alike phenomena through neural networks*, ISPRS Journal of Photogrammetry and Remote Sensing **62**(4), 2007, pp. 264–270.

[17] BREKKE C., SOLBERG A.H.S., *Classifiers and confidence estimation for oil spill detection in ENVISAT ASAR images*, IEEE Geoscience and Remote Sensing Letters **5**(1), 2008, pp. 65–69.

[18] LINLIN XU, LI J., BRENNING A., *A comparative study of different classification techniques for marine oil spill identification using RADARSAT-1 imagery*, Remote Sensing of Environment **141**, 2014, pp. 14–23.

[19] WAGNER W., PATHE C., SABEL D., BARTSCH A., KUNZER C., SCIPAL K., *Experimental 1 km soil moisture products from ENVISAT ASAR for Southern Africa*, Proceedings of ENVISAT Symposium, Montreux, Switzerland, 2007, SP-636.

[20] RAMOS-FUERTES A., MARTI-CARDONA B., BLADÉ E., DOLZ J., *Envisat/ASAR images for the calibration of wind drag action in the Doñana wetlands 2D hydrodynamic model*, Remote Sensing **6**(1), 2014, pp. 379–406.

[21] SPARWASSER N., KRAUS T., HASCHBERGER P., *Multi-temporal radar image mosaic from the Mekong River Delta (ENVISAT ASAR© ESA)*, Status Report 2007–2013, German Remote Sensing Data Center, Oberpfaffenhofen, September 2013, pp. 64–65.

[22] SHENGLI HUANG, POTTER C., CRABTREE R.L., HAGER S., GROSS P., *Fusing optical and radar data to estimate sagebrush, herbaceous and bare ground cover in Yellowstone*, Remote Sensing of Environment **114**(2), 2010, pp. 251–264.

[23] FINGAS M.F., BROWN C.E., *Review of oil spill remote sensing*, Spill Science and Technology Bulletin **4**(4), 1997, pp. 199–208.

[24] MOUCHE A.A., HAUSER D., DALOZE J.-F., GUERIN C., *Dual-polarization measurements at C-band over the ocean: results from airborne radar observations and comparison with ENVISAT ASAR data*, IEEE Transactions on Geoscience and Remote Sensing **43**(4), 2005, pp. 753–769.

[25] GIRARD-ARDHUIN F., MERCIER G., COLLARD F., GARELLO R., *Operational oil-slick characterization by SAR imagery and synergistic data*, IEEE Journal of Oceanic Engineering **30**(3), 2005, pp. 487–495.

[26] MIHOUB Z., HASSINI A., *Oil spill detection technique from RADAR and optical satellite data*, The Second International Conference on Signal, Image, Vision and their Application SIVA '13, November 18–20, 2013, Algeria, pp. 169–174.

[27] SERTAC AKAR, MEHMET LUTFI SÜZEN, NURETDIN KAYMAKCI, *Detection and object-based classification of offshore oil slicks using ENVISAT-ASAR images*, Environmental Monitoring and Assessment **183**(1–4), 2011, pp. 409–423.

[28] MIHOUB Z., HASSINI A., *Oil spill monitoring and classification technique from ENVISAT-ASAR data*, International Conference on Engineering of Industrial Safety and Environment ICISE '14, January 26–27, 2014, Algeria.

[29] WACKERMAN C.C., *Digital SAR image formation*, [In] CARSEY F.D. [Ed.], *Microwave Remote Sensing if Sea Ice*, Geophysical Monograph 68, Washington, 1992, pp. 105–110.

[30] HASSINI A., DÉJEAN S., BENABADJI N., HASSINI N., BELBACHIR A.H., *Forest fires smoke monitoring from sea-viewing wide field-of-view sensor images*, Optica Applicata **38**(4), 2008, pp. 737–754.

[31] MARGHANY M., *RADARSAT automatic algorithms for detecting coastal oil spill pollution*, International Journal of Applied Earth Observation and Geoinformation **3**(2), 2001, pp. 191–196.

[32] ÖZKAN C., SUNAR F., *Comparisons of different semi-automated techniques for oil-spill detection: a case study in Lebanon*, 27th EARSel Symposium, June 4–7, 2007, Bolzano, Italy.

[33] RUSS J.C., *The Image Processing Handbook*, CRC Press, Boca Raton, United States,1992, p. 445.

[34] ESPINDOLA G.M., CAMARA G., REIS I.A., BINS L.S., MONTEIRO A.M., *Parameter selection for region--growing image segmentation algorithms using spatial autocorrelation*, International Journal of Remote Sensing **27**(14), 2006, pp. 3035–3040.

[35] YUANMING SHU, LI J., YOUSIF H., GOMES G., *Dark-spot detection from SAR intensity imagery with spatial density thresholding for oil-spill monitoring*, Remote Sensing of Environment **114**(9), 2010, pp. 2026–3035.

Received March 3, 2014
in revised form June 1, 2014